Gyrokinetic Simulations of Turbulent Transport in a Ring Dipole Plasma

Sumire Kobayashi and Barrett N. Rogers*
Department of Physics and Astronomy, Dartmouth College, Hanover, New Hampshire 03755, USA
William Dorland†
Department of Physics, University of Maryland, College Park, Maryland 20742, USA
(Received 19 March 2009; published 30 July 2009)

Gyrokinetic flux-tube simulations of turbulent transport due to small-scale entropy modes are presented in a ring-dipole magnetic geometry relevant to the Columbia-MIT levitated dipole experiment (LDX) [J. Kesner *et al.*, Plasma Phys. J. **23**, 742 (1997)]. Far from the current ring, the dipolar magnetic field leads to strong parallel variations, while close to the ring the system becomes nearly uniform along circular magnetic field lines. The transport in these two limits are found to be quantitatively similar given an appropriate normalization based on the local out-board parameters. The transport increases strongly with the density gradient, and for small $\eta = L_n/L_T \ll 1$, $T_i \sim T_e$, and typical LDX parameters, can reach large levels. Consistent with linear theory, temperature gradients are stabilizing, and for $T_i \sim T_e$ can completely cut off the transport when $\eta \gtrsim 0.6$.

DOI: 10.1103/PhysRevLett.103.055003 PACS numbers: 52.35.Ra, 52.30.Gz, 52.65.Tt, 52.25.Fi

The Columbia-MIT levitated dipole fusion experiment (LDX) [1] confines heated plasma using a dipolar magnetic field generated by a magnetically-levitated current ring. Motivated by this experiment, we present here five dimensional gyrokinetic GS2 [2,3] flux-tube simulations of turbulent transport due to small-scale ($k_\perp \rho_i \sim 1$) entropy modes in an MHD-stable ring dipole system. The entropy mode is a plasma analogue of the thermal instability in ordinary fluids [4], modified by magnetic curvature and finite Larmor radius (FLR) effects, and early observations [5] have suggested it may indeed be active in LDX. It may also drive turbulence and transport in astrophysical systems such as planetary magnetospheres, particularly in higher-β regimes in which the possible stabilizing contribution of boundary conditions at the ionosphere (e.g., due to line-bending) may play a secondary role [6–8]. A cross section of the ring-dipole geometry and some magnetic field lines relevant to our study are shown in Fig. 1. The outer field line is located near the bulk of a typical LDX plasma and is characterized by a high mirror ratio $B_{\max}/B_{\min} \sim 37$ and high trapped particle fraction $\sqrt{1 - B_{\min}/B_{\max}} \sim 99\%$. The majority of the simulations discussed here are based on the magnetic geometry of a flux tube surrounding this outer field line and explore how the turbulence and transport at this location depend on the density and temperature gradients, the plasma collisionality, and T_e/T_i. To study how the transport depends on the magnetic geometry, we also compare simulations of the outer field line geometry in Fig. 1 to those described in our earlier work [9], which apply to flux tubes very close to the current ring. In the near-ring limit, the parallel variations and trapped particles become negligible and the field lines become circular, and therefore the system becomes equivalent to a Z pinch geometry. This comparison reveals that the normalized transport in the two limits are qualitatively and quantitatively similar, provided that the normalization in the dipole system is based on appropriate quantities at or near the outer-midplane radius R_{mid}. This normalization is preferred due to the $B \sim 1/r^3$ dipolar behavior of the magnetic field, which implies that the majority of the plasma within a flux tube is located at radii that are comparable to R_{mid}.

As a first step we consider the regime $\beta \ll 1$, in which the dominant instabilities have an electrostatic character and $k_\parallel \ll k_\perp$. As in the Z pinch system and consistent with expectations from linear theory [10], we find two main instabilities: the ideal MHD interchange mode at stronger gradients and small-scale non-MHD entropy modes at weaker gradients. The local linear growth rate for the ideal mode can be written as [10]:

$$\frac{\gamma_{\mathrm{ideal}}}{\langle \omega_{di} \rangle_\theta} \approx \sqrt{\frac{d - \frac{10}{3}}{\langle b_i \rangle_\theta}} \tag{1}$$

where $d \equiv \frac{2\omega_{*i}(1+\eta)}{\langle \omega_{di} \rangle_\theta} = -2\frac{dlnp}{dlnU} \sim R/L_p$ is a measure of the pressure gradient, $b_i \equiv (k_\perp^2 T_i/Z_i m_i \Omega_{ci}^2) \ll 1$, $\omega_{*i} \equiv \frac{clT_i}{Z_i e n_0}\frac{dn_0}{d\psi}$, $\langle \omega_{di} \rangle_\theta = -\frac{clT_i}{Z_i eU}\frac{dU}{d\psi}$, $\eta \equiv \frac{dlnT_i(\psi)/d\psi}{dlnn_0(\psi)/d\psi} = L_n/L_T$,

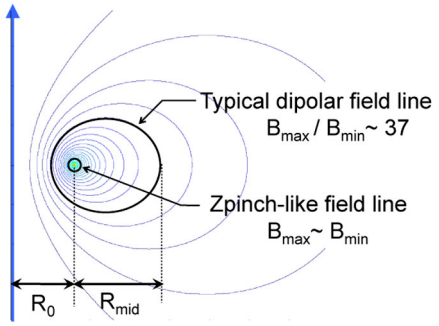

FIG. 1 (color online). Ring-dipole magnetic flux tubes.

$\langle \cdots \rangle_\theta = U^{-1} \oint [(\cdots) d\theta/(\mathbf{B}\cdot\nabla\theta)]$, $U(\psi) \equiv \oint [d\theta/(\mathbf{B}\cdot\nabla\theta)]$, ψ is flux function, n_0 is background density, L_n, L_T are background density and temperature gradient scale lengths, and $\oint d\theta$ is an integral along a flux tube. The system is stable to ideal interchange modes when the gradients are sufficiently weak: $d < 10/3$. Here we focus on such ideally stable regimes, in which the dominant instability is the entropy mode. For a $T_i = T_e$ equilibrium and $k_\perp \rho_i \ll 1$, the entropy growth rate is given by [10]:

$$\frac{\gamma_{\text{entropy}}}{\langle \omega_{di} \rangle_\theta} = \sqrt{\frac{5(d\frac{7-3\eta}{1+\eta} - 10)}{9(\frac{10}{3} - d)}}. \quad (2)$$

This expression predicts the mode is unstable for $10/7 < d < 10/3$ when $\eta = 0$, while for finite η, stability for any $d < 10/3$ is reached when $\eta > 2/3$. This cutoff with increasing η, as we show later, is consistent the GS2 code, although for small η the code predicts instability even below $d < 10/7$. Figure 2 shows linear entropy mode growth rates obtained numerically using GS2 for various d values, $T_i = T_e$, $\eta = 0$, and weak collisionality. The plots in this article refer to a coordinate system (x, y, z) in which the z direction is parallel to the magnetic field. The x and y directions are both perpendicular to $\vec{B}$ and to each other, with y representing the ignorable (toroidal) coordinate around the symmetry axis of the device and the x direction aligned parallel to the plasma gradients (i.e., radial at the outer midplane). As in the Z pinch limit [9], Fig. 2 shows the entropy mode growth rates remain robust up to remarkably high values of $k_y \rho_i$ (here and elsewhere, unless otherwise noted, ρ_i is evaluated at the outer midplane of the outer field line shown in Fig. 1). The quantitative similarity of Fig. 2 to the Z pinch case, which exhibits roughly comparable peak growth rates at $k_\perp \rho_s \sim 1$ [$\rho_s = c_s/\Omega_{ci}$, $c_s^2 = (T_i + T_e)/m_i$], depends strongly on the normalization in the dipole case. Normalizing γ and k_y to the inboard rather than outboard midplane parameters, for example, increases the normalized growth rates by about a factor of 10 and shifts the peak of the k spectrum down to $k_\perp \rho_s \sim 1/37 \sim 0.03$.

Turning to the nonlinear regime, the simulations include 128×128 Fourier modes in the x and y directions spanning the range $0.27 \le k_\perp \rho_i \le 17$, 32 grid points in the parallel (z) direction, 24 ion and 24 electron energy grid points in the velocity space region $0 \le v \le 6 v_{\text{thi}}$, and 10 grid points in $\xi = v_\parallel / v$. Simulations have been carried out to verify the insensitivity of the transport values reported here to variations in the spatial and velocity space resolutions and box size. The mass ratio is $m_i/m_e = 3672$ (deuterium) and the collision frequency is defined as $\nu_{\text{phys}} = \pi n_0 e^4 \ln\Lambda/(T_i^{3/2} m_i^{1/2}) \equiv \nu\sqrt{2} v_{\text{thi}}/R_{\text{mid}}$. Collisions in the code are modeled by a gyro-averaged Lorenz collision operator [11] that conserves total energy and particle number. We also conducted several simulations with a more refined collision operator [12] that includes energy diffusion and conserves momentum and confirmed that the transport dynamics are qualitatively and quantitatively similar. The more refined operator, however, was not operational across the full range of parameters explored here, and further code development is required to complete the comparison. No numerical hyperviscosity was used.

Figure 3 shows the progression of the electrostatic potential in a GS2 simulation at a moderate density gradient ($d = 1.25$, $\eta = 0$) and either low collisionality [Figs. 3(a)–3(c) $\nu = 0.0000015$]or high collisionality [Fig. 3(d), $\nu = 0.15$]. Unless otherwise noted, the plots show ϕ at the outer midplane perpendicular to the magnetic field with the horizontal coordinate x directed radially outward and the vertical coordinate y directed toroidally, around the symmetry axis. Plots of ϕ at other locations along the flux tube such as the inner midplane look nearly identical. Following initialization with low-amplitude random noise (not shown), the fastest growing entropy modes, visible as the horizontal streamers in Fig. 3(a), eventually dominate with $k_y \rho_s \sim 1$ and $k_x = 0$. Exponential growth of the entropy mode spectrum continues until nonlinear saturation, which is triggered by the onset of the Kelvin-Helmholz instability (KHI) with $k_x \rho_i \sim 0.5$ as shown in Fig. 3(b). These two plots are representative of essentially all the parameter regimes considered in this study. Following this, however, the nonlinear development of the KHI leads to sheared $\mathbf{E} \times \mathbf{B}$ flows in the y direction, and the damping and stability of these zonal flows depends on the parameters ν and d. At moderate to weak gradients (e.g., $d \lesssim 1.34$) and low collisionality, the late-time zonal flows are undamped and robustly stable [see, e.g., Fig. 3(c) for $\nu = 0.000015$]. The corresponding particle and heat trans-

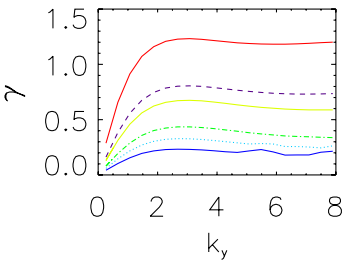

FIG. 2 (color online). γ vs $k_\perp$ (normalized to $v_{\text{thi}}/R_{\text{mid}}$ and $1/\rho_s$, respectively) for $\eta = L_n/L_T = 0$, $\nu = 0.000015$ and (bottom to top): $d = 1.25, 1.34, 1.49, 1.75, 1.89, 2.22$.

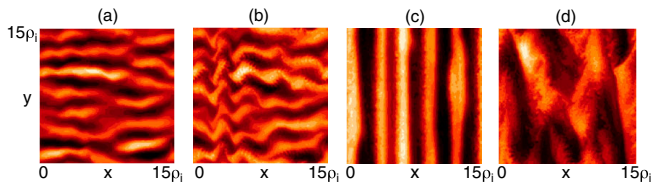

FIG. 3 (color online). Snapshots of ϕ for $d = 1.25$, $\eta = 0$ at the outboard midplane showing (a) linear phase, (b) onset of the KHI, and (c) the late-time behavior for low collisionality, $\nu = 0.0000015$ or (d) high collisionality, $\nu = 0.15$.

port levels are very small, as can be seen from the red (triangle) curves in Figs. 4(a)–4(c). (The fluxes are normalized $(\rho_s/R_{\rm mid})^2 v_{\rm thi} f$ with $f = n_0$ for the particle flux and $f = n_0 T_\alpha$ for the heat fluxes, and the plots are for $\eta = 0$. The ion and electron particle fluxes are equal to the level of numerical accuracy of the code.) In contrast, at moderate to weak gradients but high collisionality, the zonal flows are damped by the collisions and plots of ϕ look much more turbulent (see, e.g., Fig. 3(d) for $\nu = 0.15$). The transport levels are correspondingly higher at large ν [see, e.g., the green (open rectangle) curves in Figs. 4(a)–4(d) for $\nu = 0.15$], despite a reduction in this limit of the linear growth rates at high $k_\perp$. This behavior is also consistent with Fig. 4(d), which shows the time-averaged root-mean-square (RMS) shearing rates $V' = dv_{E,y}/dx$ due to the six longest-wavelength zonal flow modes in the system (our tests show that the smaller wavelength zonal flows do not substantially impact the transport). The range of linear growth rates γ are also shown in blue (light dots). Except at the steepest gradients (highest d), the shearing rates are higher than the γ values at small $\nu = 0.000015$ [red (triangle) curve] and are comparable to γ at high $\nu = 0.15$ [green (open rectangle) curve].

These features persist as the density gradient $\propto d$ is increased up to about $d \sim 1.9$, at which point the quasi-static zonal flows, like those shown in Fig. 3(c) for small ν, become unstable. In this steeper gradient regime the simulations are turbulent and appear qualitatively and quantitatively similar regardless of the collisionality. As in the Z pinch case, we believe this is due to the emergence of (tertiary) Kelvin-Helmholz instabilities of the zonal flows, which replace the collisional damping as the main regulator of the zonal flow amplitudes as V_E' in the simulations increases with d. It is difficult to identify a precise Kelvin-Helmholtz stability threshold due to the coupling of the KHI to the (unstable) entropy mode at low frequencies. As the velocity shear V_E' due to the zonal flow modes in the simulations is artificially increased, for example, the linear growth rates and nonlinear transport levels typically decrease at first, presumably due to the stabilizing impact of V_E' on the entropy modes. At still higher values of V_E', however, the trend reverses and the transport and growth rates start to slowly increase, presumably due to the emergence of the Kelvin-Helmholz instability. What is clear is that at weak gradients the zonal flows in the nonlinear simulations are immune to the KHI, while they become strongly unstable if their amplitudes are sufficiently increased. The orange (solid) curve in Fig. 4(d) shows the latter V_E' limit at which robust Kelvin-Helmholz modes are visible. This curve, which likely somewhat overestimates the V_E' threshold, was obtained using the method illustrated in Fig. 5. This figure shows the behavior of the zonal flow modes at steep gradients ($d = 2.22$) when they are increased by a factor of 1.8 upon restart, with the other modes in the simulation reset initially to small levels. Figure 5(a) shows the ϕ profile upon restart and Fig. 5(b) shows the subsequent onset of the KHI, identifiable by its wavelength in the y direction, which is comparable to scale of the background zonal flows and is substantially longer than those typical of entropy modes. The drop in the orange (solid) curve in Fig. 4(d) as d is increased is possibly due to the coupling of the KHI to the (stable) ideal interchange mode [9], which becomes progressively weaker as the ideal marginal stability boundary at $d = 10/3$ is approached.

As can be seen from Fig. 6(a), in contrast to the destabilizing effect of the density gradient, temperature gradients (in the same direction as the density gradient) are stabilizing for entropy mode turbulence. In the simulations of Fig. 6(a) the density gradient was held fixed and η was increased such that $d = 1.89(1 + \eta)$. Consistent with the predictions of linear theory [13] the transport cuts off at about $\eta \sim 0.6$. This cutoff may have important experimental consequences for LDX, given that the experiments typically operate with finite $\eta > 0$, and given that the predicted entropy mode transport for LDX parameters can be quite large for $\eta = 0$. For example, defining $\Gamma_{\rm phys} \equiv n v_{\rm eff}$ and considering deuterium plasma parameters with $T_e \sim T_i \sim 100$ eV, $R_{\rm mid} \sim 0.5$ m $B_{\rm mid} \sim 0.2T \propto 1/R_{\rm mid}^3$, the normalized GS2 particle flux $\Gamma_{\rm GS2}$ plotted

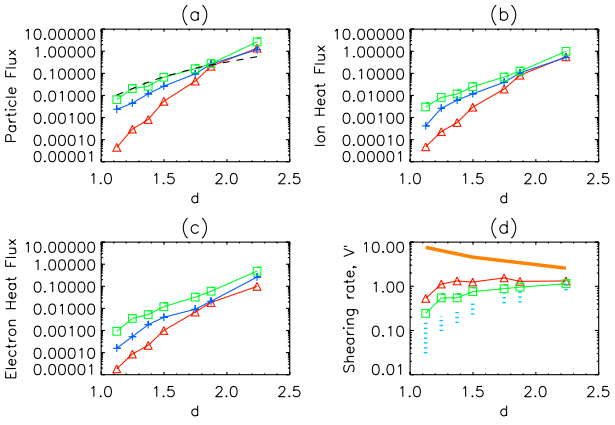

FIG. 4 (color online). (a) $\Gamma_{\rm part}$ for $\nu = 0.000015$ (red triangles), 0.0015 (blue crosses), 0.15 (green open rectangles), and a mixing length estimate (dashed black). (b),(c) The ion and electron heat fluxes. (d) The corresponding RMS shearing rates V_E' and $\gamma_{\rm entropy}$ (light blue dots) and an approximate KHI threshold (orange solid).

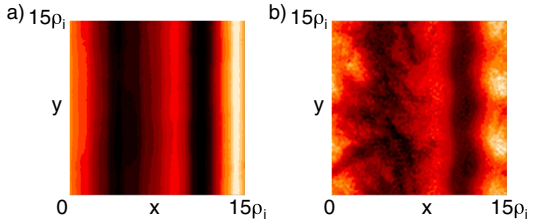

FIG. 5 (color online). The KHI when the zonal flows are amplified by 1.8 times for $d = 2.22$ (a) at restart and (b) after $t \sim 5R_{\rm mid}/v_{\rm thi}$.

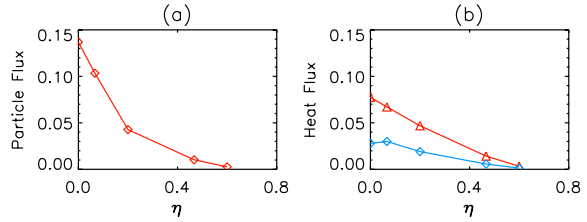

FIG. 6 (color online). (a) Particles flux (ion and electrons same) and (b) ion (red triangles) and electron (blue diamonds) heat flux versus η for $\nu = 0.000015$.

in Fig. 4(a) yields $v_{\rm eff} \sim \Gamma_{\rm GS2} v_{\rm thi} (\rho_{i,\rm mid}/R_{\rm mid})^2 \sim \Gamma_{\rm GS2} 10 \Gamma_{\rm GS2} (T_i/100\ {\rm eV})^{3/2} (R/0.5\ {\rm m})^4 \sim 10 \Gamma_{\rm GS2}$ m/s, where $\Gamma_{\rm GS2} \sim 1$ and larger for $\eta = 0$ and density gradients that are about 30% below ideal marginal stability and steeper ($d \gtrsim 2.2$). Equivalently, $D \sim \Gamma_{\rm phys}/n_0' \sim v_{\rm eff} L_n$ where $L_n \sim 0.3$ m. These results suggest the operational space of an LDX-like device may be limited by entropy mode turbulence either to the regime $\eta \gtrsim 0.6$ (which seems potentially accessible since the entropy mode heat fluxes are nominally smaller than the particle fluxes), or else the density profile will remain stiffly clamped by the transport to gradients moderately below ($\sim 1/2$–$2/3$) the ideal interchange stability limit.

Expectations based on linear theory, calculated either with GS2 or Eq. (27) of Ref. [10], are also roughly consistent with an observed increase in the transport levels with increasing T_e/T_i. Figure 7 shows this dependence at a steep density gradient $d = 2.2$ and $\eta = 0$. Relative to the $T_e = T_i$ case, the particle transport is reduced by about factor of 2 for $T_e/T_i = 1/3$, and increased by a factor of ~ 3.1 for $T_e/T_i = 3$.

Turning finally to the dependence of the turbulence and transport on the geometry and location of the flux tube, we note two key facts: First, the fluxes in the dipole system typically exhibit strongly enhanced values at the outboard midplane relative to the inboard midplane (a factor of $\sim 60 \sim 2B_{\rm max}/B_{\rm min}$ at the steepest gradients, and smaller collisionality-dependent amounts at weaker gradients). This asymmetry is due mainly to the $1/B$ dependence of the (radial) $\vec{E} \times \vec{B}$ velocity. The second fact is that the *total* transport levels, when normalized to the outboard midplane parameters, do *not* depend strongly on the location

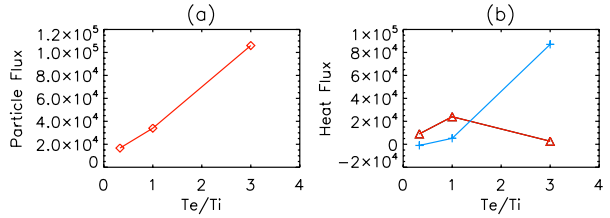

FIG. 7 (color online). (a) Particles flux (ion and electrons same) and (b) ion (red triangles) and electron (blue crosses) heat flux versus T_e/T_i for $\eta = 0$ and $\nu = 0.000015$.

of the flux tube: the normalized transport levels shown in Fig. 4, for example, are comparable to, or at higher gradients somewhat less than (e.g., by about a factor of 3), those found previously in the Z pinch limit [9]—a limit that, in our system, applies to flux tubes very close to the current ring. The factor of 3 reduction might reflect our relatively extreme choice of outboard-midplane normalizing parameters: choosing values that are radially about $\sim 30\%$ closer to the ring would boost the normalized transport in the dipole system by about a factor of ~ 3. (In contrast, normalizing the transport to plasma parameters at the inner midplane would yield a factor of ~ 1400 increase.) With an outboard midplane normalization, the mixing length argument for the transport described in the Z pinch system [9] also roughly applies here, at least in the higher ν simulations in which the zonal flows are not a dominating factor. Normalizing ϕ to $T_i \rho_i/(eR_{\rm mid})$, γ to $v_{\rm thi}/R_{\rm mid}$, $k_\perp$ to $1/\rho_i$, and n to $n_0 \rho_i/R_{\rm mid}$, we estimate $\phi \sim \gamma/k_\perp^2$, and from the continuity equation, $n \sim \phi$, so that $\Gamma_{\rm part} \sim k_\perp \langle n\phi \rangle \sim \gamma^2/k_\perp^3$. Choosing $k_\perp \rho_i \sim 0.4$, a value that typically contributes strongly to the transport, this estimate is shown as the black dashed curve in Fig. 4(a). A similar estimate applies to the heat flux, which displays a comparable parametric trend.

In conclusion, small-scale entropy mode turbulence driven by the entropy mode in a ring-dipole system exhibits a large variation of the turbulent transport as a function of the density gradient (which is destabilizing) and temperature gradient (stabilizing). Normalizing the transport to local plasma parameters at the outer midplane, robust transport is observed when $T_0' = 0$ and n_0' is within about a factor of $1/2$ to $2/3$ of the ideal MHD interchange stability limit. Consistent with linear theory predictions, the transport cuts off when $\eta \sim 0.6$ or larger and, when the density gradient is steep, tends to increase with T_e/T_i.

This research was supported by grants from the US DOE and NERSC. We thank Dr. P. Ricci and Dr. T. Tatsuno for useful suggestions regarding the use of GS2.

*sumire.kobayashi@dartmouth.edu, barrett.rogers@dartmouth.edu
†bdorland@umd.edu

[1] J. Kesner *et al.*, Plasma Phys. Rep. **23**, 742 (1997).
[2] M. Kotschenreuther *et al.*, Comput. Phys. Commun. **88**, 128 (1995).
[3] W. Dorland *et al.*, Phys. Rev. Lett. **85**, 5579 (2000).
[4] A. A. Ware, Nucl. Fusion Suppl. **3**, 869 (1962).
[5] D. T. Garnier *et al.*, J. Plasma Phys. **74**, 733 (2008).
[6] H. Wong *et al.*, Phys. Plasmas **8**, 2415 (2001)
[7] W. Horton *et al.*, J. Geophys. Res. **104** 22 745 (1999).
[8] A. Chan *et al.*, J. Geophys. Res. **99**, 17 351 (1994).
[9] P. Ricci *et al.*, Phys. Rev. Lett. **97**, 245001 (2006).
[10] A. Simakov *et al.*, Phys. Plasmas **8**, 4414 (2001).
[11] P. Ricci *et al.*, Phys. Plasmas **13**, 062102 (2006).
[12] M. Barnes *et al.*, Phys. Plasmas **16**, 072107 (2009).
[13] J. Kesner *et al.*, Nucl. Fusion **41**, 301 (2001).